Seasonally dependent interannual variability of sea ice in the Bering Sea and its relation to atmospheric fluctuations

Yoshi N. Sasaki and Shoshiro Minobe

Division of Earth and Planetary Sciences, Graduate School of Science, Hokkaido University, Sapporo, Japan

Received 14 May 2004; revised 22 February 2005; accepted 14 March 2005; published 18 May 2005.

[1] Interannual variability of sea ice in the Bering Sea and its relationship to atmospheric variability is analyzed using a singular value decomposition (SVD) analysis of sea ice concentrations (SICs) and 1000 hPa wind speeds in winter and spring seasons. The statistically significant first and second SVD modes, explaining 76.3% and 17.6% in winter and 54.6% and 29.6% in spring of the squared covariance between the two fields, are identified for SICs both in the winter and spring seasons with 1 month leading wind speeds. The spatial structures show that the first (second) SVD mode explains the SIC variability in the northeastern (northwestern) Bering Sea, related to the local northwesterly (northerly) wind anomalies for the positive SIC anomalies both in the winter and spring seasons. A comparison of the first SVD modes between the winter and spring seasons suggests that the difference of dominant patterns of wind anomalies results in the difference of SIC anomaly distributions between two seasons. The relationship between sea ice and atmospheric circulation anomalies indicates that one mode of the leading two SVD modes in each season is related to large-scale atmospheric circulation associated with the Aleutian low and the other mode is related to relatively local atmospheric fluctuations related with pressure anomalies over Alaska. Furthermore, a slight difference of 700 hPa geopotential height anomalies results in the substantially different sea ice anomalies. These results suggest that in order to know the interannual sea ice variability in the Bering Sea, a better understanding of the wind anomalies over the Bering Sea are important.

Citation: Sasaki, Y. N., and S. Minobe (2005), Seasonally dependent interannual variability of sea ice in the Bering Sea and its relation to atmospheric fluctuations, *J. Geophys. Res.*, *110*, C05011, doi:10.1029/2004JC002486.

1. Introduction

[2] Year-to-year variability of sea ice in the Bering Sea, whose topography is shown in Figure 1, is an important scientific issue for global climate changes [e.g., *Wang and Ikeda*, 2000; *Parkinson and Cavalieri*, 2002] and also for regional environmental changes [e.g., *Stabeno et al.*, 2001]. Several studies investigated the relation between the sea ice and atmospheric parameters for the year-to-year sea ice variability of the Bering Sea. Analyzing sea level pressures (SLPs), *Walsh and Sater* [1981] suggested that when northerly wind anomalies occurred, the sea ice area tends to be large. *Niebauer* [1980] reported that greater than normal sea ice extent is accompanied by northerly component of local surface winds. *Overland and Pease* [1982] suggested that the frequent storms in the eastern (western) Bering Sea are related to a larger (smaller) sea ice extent. *Fang and Wallace* [1998] showed that the out-of-phase relation of sea ice extent between the Bering and Okhotsk Seas is held on interannual timescales in association with the western Pacific (WP) pattern in 500 hPa heights leading the sea ice by a month. When the sea ice concentration (SIC) anomalies in the Bering Sea are positive, the WP pattern is negative (500 hPa height anomalies over Kamchatka Peninsula are positive, and those over Japan are negative). The negative WP pattern is accompanied by northerly wind anomalies over the Bering Sea, consistent with other studies. *Cavalieri and Parkinson* [1987] reported that the sea ice extent in the Bering Sea tends to be out of phase with the sea ice extent in the Okhotsk Sea on intraseasonal timescales. These studies suggest that wind anomalies over the Bering Sea play a dominant role in the year-to-year sea ice variations.

[3] Interannual sea ice changes may be caused by either dynamic or thermodynamic mechanisms, and in both the mechanisms, wind anomalies may play central roles. The dynamic mechanism is wind drag of the sea ice. It is known that sea ice in the open ocean moves sea ice at an angle of 30° to the right of surface wind direction at about 4% of the wind speed at 3 m [*Reynolds et al.*, 1985]. Recently, *Kimura and Wakatsuchi* [2000, 2001] showed that ice motions are well explained by the wind drag in the Bering Sea, based on daily satellite observations. For the thermodynamic mechanism, winds may contribute to the anomalous sea ice formations via heat flux anomalies; northerly winds bring cold and dry airs onto the Bering Sea, and hence enhances the ocean-to-atmosphere heat fluxes, which can result in greater ice formations.

0148-0227/05/2004JC002486$09.00

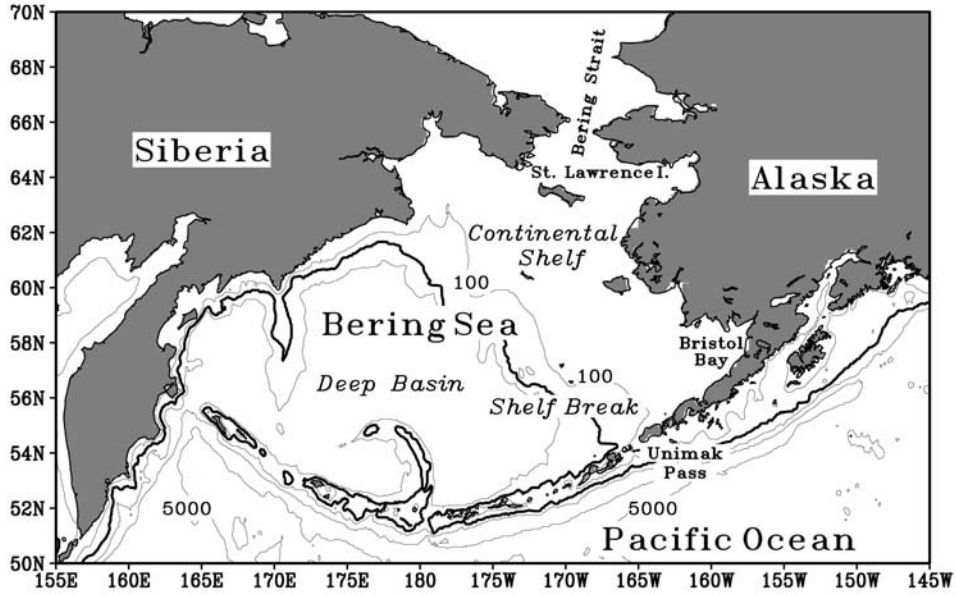

Figure 1. Bathymetry of the Bering Sea. The contour levels are 100, 1000, 3000, and 5000 m depths, with the thick contour for 1000 m depth.

[4] However, the relation between the sea ice in the Bering Sea and wind anomalies are not fully understood. Are the year-to-year sea ice variations in the Bering Sea explained by a single pattern of wind anomalies, or by physically meaningful two or more patterns? *Fang and Wallace* [1998] studied the relation between SIC anomalies and geopotential height anomalies over the Northern Hemisphere by using a singular value decomposition (SVD) analysis, and documented only one mode. Although the geopotential heights are useful in order to know hemispheric-scale atmospheric circulation anomalies, geopotential heights may have rather indirect physical relationship to the sea ice field than surface wind speeds. Thus if one examines wind speed anomalies, instead of geopotential height anomalies, one may find different and physically more direct relations to the sea ice. In particular, relations between the wind speeds and sea ice may emphasize localized structures, because the wind speed anomalies are roughly proportional to the spatial derivatives of geopotential height anomalies, and a spatial derivative is a kind of high-pass filter. Consequently, the wind anomalies contain relatively stronger energy on short-spatial-scale phenomena than the geopotential heights. The Bering Sea, which is the third largest marginal sea in the world, might have physically and statistically meaningful two or more modes between the sea ice and atmospheric parameters. If this is the case, to identify those modes is of clear scientific value. Therefore we investigate the relation between the sea ice and atmospheric parameters, by using a SVD analysis between SICs and wind speed anomalies at the 1000 hPa geopotential heights.

[5] Furthermore, in order to know the seasonal dependency of year-to-year sea ice variability, we examine winter (December–February) and spring (March–May) SICs separately. In the winter and spring seasons, the sea ice prevails over the shallow continental shelf and around the shelf break mainly in the northeastern Bering Sea, with the 20% contour line of climatological SICs roughly corresponding to the shelf break in the northern Bering Sea (Figure 2). The SIC averaged over the Bering Sea reaches its maximum in

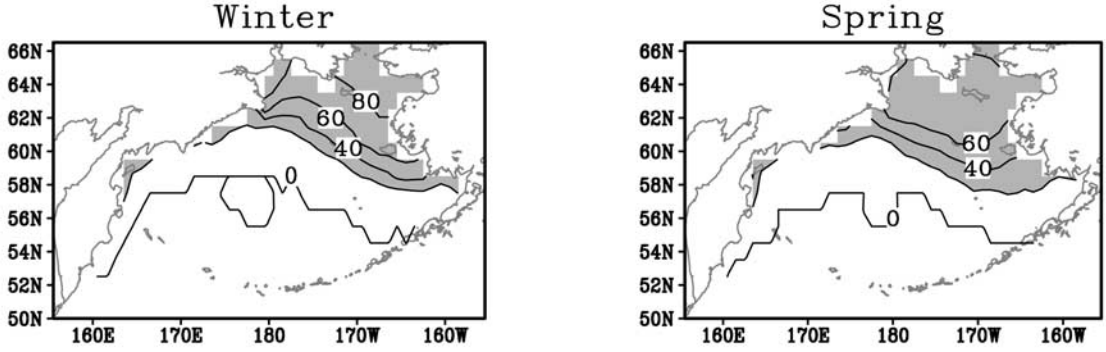

Figure 2. Climatology of sea ice concentration (SIC) in winter and spring seasons. The contour interval is 20%, and the regions where the climatologies are larger than 20% are shaded.

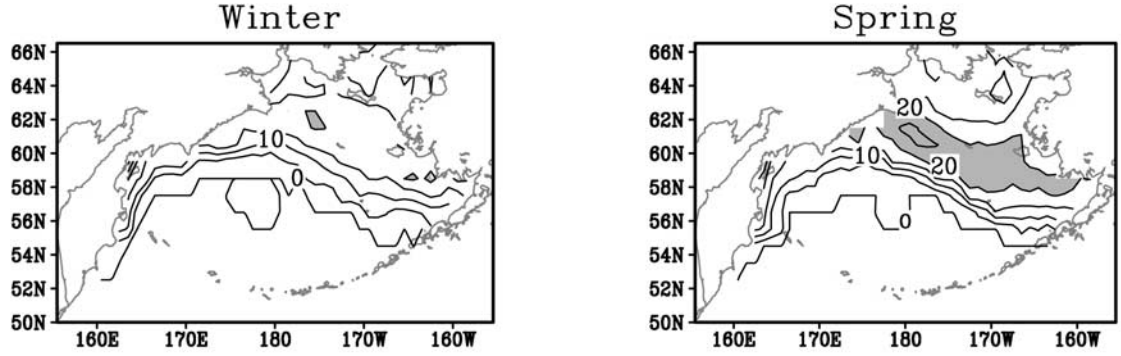

Figure 3. Standard deviation of SIC anomalies in winter and spring seasons. The contour interval is 5%, and the regions where the standard deviations are larger than 20% are shaded.

March, and hence the winter and spring seasons correspond climatological ice-increasing and ice-decreasing seasons, respectively. The Bering Sea is virtually ice-free in the summer and autumn seasons. The year-to-year variability of SICs, expressed by interannual standard deviation, are larger in the spring season than in the winter season (Figure 3), with the standard deviations averaged over the Bering Sea reaching their maximum in April [*Parkinson*, 1991]. The patterns of the standard deviation indicate that the topography also influences the interannual variability of the SICs, as the strong year-to-year variability of SICs is observed in the southern part of the continental shelf and around the shelf break. It is noteworthy that the Bering Sea marine ecosystem is characterized by the highly productive area known as "Bering Sea Greenbelt" along the shelf break [*Springer et al.*, 1996], and sea ice in spring plays an important role in the spring bloom of phytoplankton [e.g., *Niebauer et al.*, 1990; *Saitoh et al.*, 2002; *Hunt and Stabeno*, 2002]. Thus the year-to-year sea ice variability might play a role in the Bering Sea ecosystem.

[6] The rest of the present paper is organized as follows. In section 2, data and methodology are explained. The results are described in section 3, with subsections of the relation between sea ice and surface wind, and the relation between sea ice and atmospheric circulation. Summary and discussion are presented in section 4.

2. Data and Method

[7] A monthly SIC data set on a $1^\circ \times 1^\circ$ grid from 1870 to 2003 is provided from the UK Meteorological Office as the Hadley Centre sea ice and sea surface temperature data set version 1 (HadISST1). Detailed methodologies for the production of HadISST1 are described by *Rayner et al.* [2003]. In HadISST1, the SICs between 1901 and October 1978 are mainly derived from Walsh's data [*Walsh and Johnson*, 1979; *Walsh and Chapman*, 2001], and which incorporated satellite observations after 1972 [*Walsh and Chapman*, 2001]. The passive microwave SICs data from November 1978 to 1996 are derived from the Goddard Space Flight Center [*Cavalieri et al.*, 1999], and from 1997 onward are derived from the NCEP [*Grumbine*, 1996]. However, the SICs in HadISST1 for the period 1940–1952 are set to the calendar monthly 1940–1952 climatology [*Rayner et al.*, 2003]. Because the SICs from 1940 to 1952 are set to the calendar monthly climatology, we use the data after 1953. We analyze the data in a rectangle region (52.5°–66.5°N, 155.5°E–155.5°W) roughly corresponding the Bering Sea, and filled SICs outside of the Bering Sea with missing values.

[8] Monthly atmospheric data, including 1000 hPa wind speeds, 700 hPa geopotential heights (Z700), 1000–500 hPa thickness, and surface air temperature (SAT) are taken from the NCEP/NCAR reanalysis data set [*Kalnay et al.*, 1996]. The data have a global coverage gridded on a $2.5^\circ \times 2.5^\circ$ grid from 1949 to 2003, but only the SAT data have a T62 Gaussian grid (roughly 1.90° latitude $\times$ 1.875° longitude grid).

[9] The major analysis method in this study is a SVD analysis [*Bretherton et al.*, 1992], which can extract covariability between two fields. We conduct a SVD analysis based on a covariance matrix constructed from the yearly sampled seasonally averaged (winter or spring) anomalies, with weights proportional to the area represented by grid. The zonal and meridional wind speeds are combined, so that the covariance matrix has the size of (N, $2M$), where N is the number of grids for the SICs and M is the number of grids for the wind speeds. We analyze the 1000 hPa wind speed data only over the Bering Sea (50°N–70°N, 155°E–145°W). Previous studies suggest that interannual sea ice variability lags atmospheric variability by 2–6 weeks [e.g., *Fang and Wallace*, 1998; *Deser et al.*, 2000]. Thus for the calculation of the SVD modes for the winter (December–February) SICs, we use 1 month leading (November–January) wind speed data. Similarly, the SVD modes for the spring (March–May) SICs are calculated with the February–April wind speeds. We also examined 2 month lag or zero month lag, but found that the 1 month lag (atmosphere-leading) gives the highest covariability between the two fields. In this paper, winter has been defined as December, January and February and is labeled by the year for the appropriate January, and spring has been defined as March, April and May. Accompanied patterns of atmospheric circulation are determined by a regression analysis of Z700, 1000–500 hPa thickness and SAT onto the temporal coefficients of the SVD mode.

[10] The representativeness of a SVD mode is examined by several measures. First, squared covariance is the square of the covariance explained by a SVD mode. Second, squared covariance fraction (SCF) is the ratio of the squared covariance explained by a SVD mode to the total squared covariance. Third, correlation coefficient between the tem-

poral coefficients of the two fields of a SVD mode indicates how the two fields are tightly related. The last measure is variance fraction (VARF), which is the ratio of the explained variance of a field relative to the total variance of a field. Here, the explained variance is calculated based on heterogeneous regression coefficients. If we assume one independent observation per each year in the 51 year data, the significant correlation coefficient at the 95% (99%) confidence level is 0.28 (0.36).

[11] In order to access the robustness of the SVD modes, we estimate the statistical significance of the squared covariance using a Monte Carlo test [*Venegas et al.*, 1997]. We conduct 300 sets of SVD analyses between the SICs and temporally shuffled 1000 hPa wind speeds. When the observed squared covariance is larger than the top 1% of the surrogate squared covariances, the SVD mode is regarded to be significant at the 99% confidence level. In winter, the Monte Carlo test shows that the leading two modes are significant, while in spring the leading three modes appeared to be significant. Thus single mode is not sufficient to explain the relation between the SIC and wind anomalies for the third largest marginal sea in the world, but at least two modes should be take into account. Yet, the third SVD mode in spring explains small variability of sea ice (5.0%), this mode can be ignored practically. Therefore we show the results of the first SVD mode (SVD-1) and the second SVD mode (SVD-2) both in the winter and spring seasons. We also examined winter and spring SICs by an empirical orthogonal function (EOF) analysis, and found that the leading two EOF modes in the winter and spring seasons are essentially the same as those obtained by the SVD analysis.

[12] The quality of the SIC data may present some problems before 1972 when satellites data were not available. Therefore in order to check the quality of the SIC data and how stable the SVD results, we also perform the SVD analyses separately for the period 1953–1971 and 1972–2003. The result shows that the leading two SVD modes before 1972 and after 1972 and from 1953 to 2003 are essentially same, although the relationship between SICs and wind speed of the SVD modes before 1972 are weaker than those after 1972 and the ordering of the leading two modes is opposite in the wintertime SVD analysis before 1972 compared to those after 1972 and from 1953 to 2003. Because the leading two SVD modes for the three different periods are essentially same, we use the data from 1953 to 2003 in the present paper.

3. Results

3.1. Relation Between Sea Ice and 1000 hPa Wind

[13] Figure 4 shows the heterogeneous regression maps and the temporal coefficients of the first SVD mode between winter mean (December–February) SIC anomalies and November–January mean 1000 hPa wind speed anomalies. The heterogeneous regression map for SIC as shown in Figure 4a exhibits large positive amplitudes around the shallow shelf in the northeastern Bering Sea, and these positive anomalies are located around the eastern part of the area where the standard deviations of SIC anomalies are large (Figure 3). The explained variance calculated based on heterogeneous regression coefficients

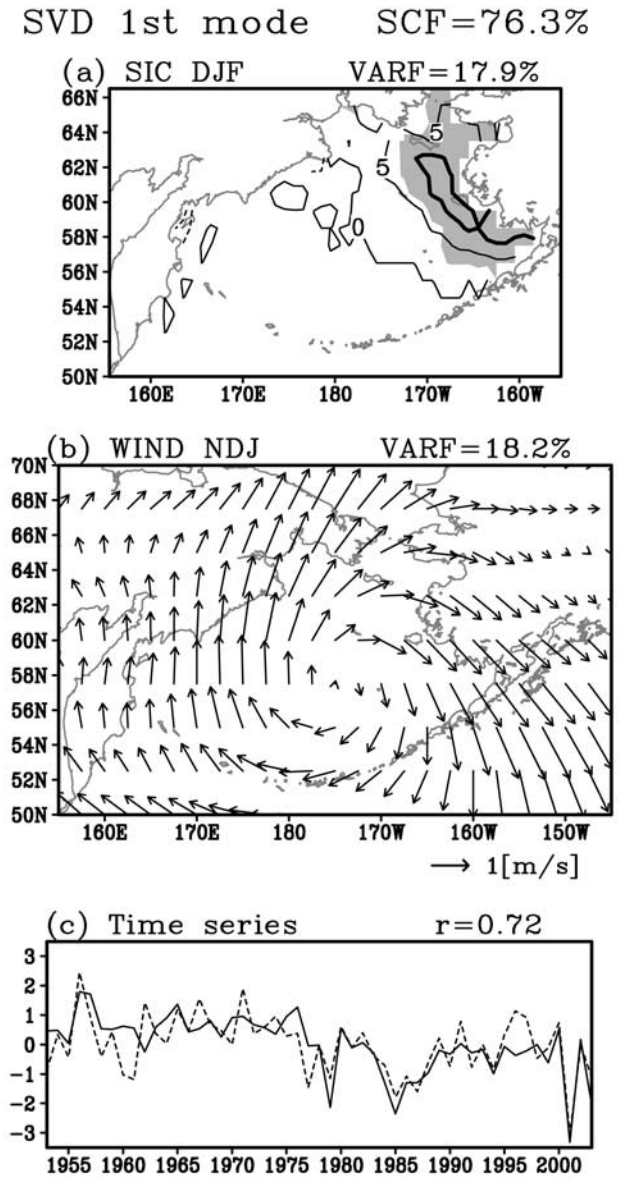

Figure 4. First singular value decomposition (SVD) mode of the wintertime SICs from December to February and 1 month leading 1000 hPa winds from November to January from 1953 to 2003. (a) Heterogeneous regression map for SIC. The contour interval is 5%, and the thick contour indicates 10%. The regions where the absolute values of corresponding correlation coefficients are larger than 0.4 are shaded. (b) Heterogeneous regression map for 1000 hPa wind. Scaling for the vectors is given at the lower-right corner. (c) Time series of the normalized temporal coefficients for SIC (solid curve) and 1000 hPa wind (dashed curve).

is 17.9% and based on homogeneous regression coefficients, which corresponds to the explained variance of an EOF mode, is 38.8% (not shown).

[14] The heterogeneous regression map for 1000 hPa wind indicates anticyclonic wind anomalies around the center of the Bering Sea (Figure 4b). Northwesterly and west-northwesterly wind anomalies prevail over the large

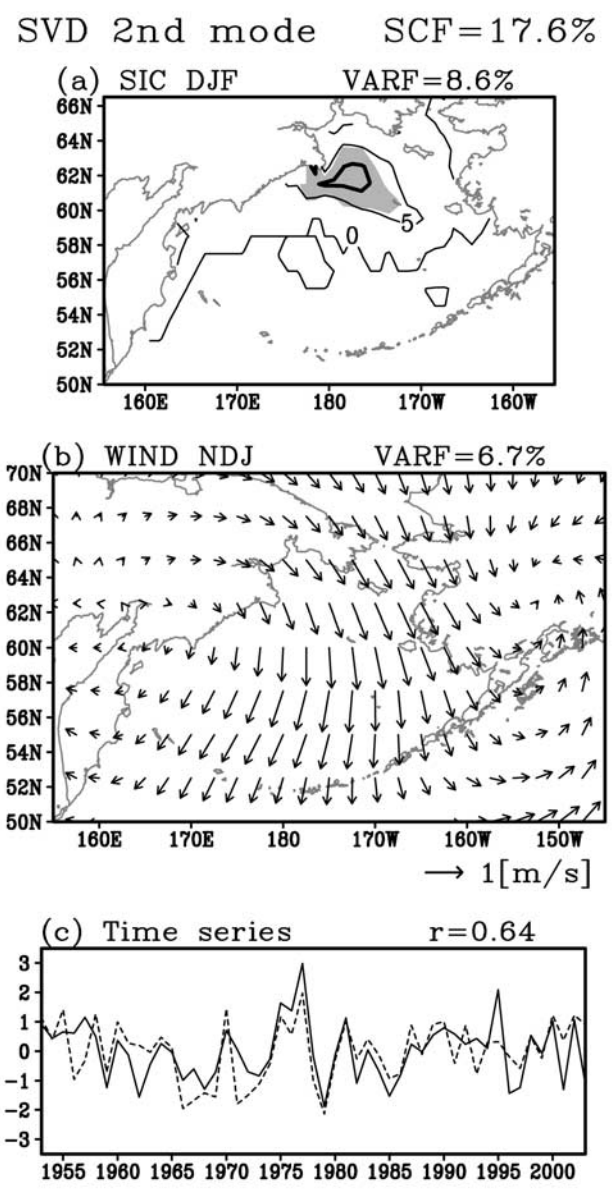

Figure 5. Same as Figure 4, but for the second SVD mode.

SIC positive amplitudes. This result indicates that the anticyclonic wind anomalies are related to the positive sea ice anomalies in the northeastern Bering Sea. This relationship can be explained either by the dynamic mechanism (sea ice drift) or by the thermodynamic mechanism (ice formation due to heat fluxes); the northwesterly and west-northwesterly wind anomalies can directly drag sea ices with larger SICs from the north, or bring colder air masses, which increase surface heat fluxes from the ocean, resulting larger SICs. Furthermore, convergences (divergences) of wind anomalies produce sea ice convergences (divergences).

[15] The temporal coefficients for SIC (Figure 4c), which are well correlated to area-averaged SICs over the whole Bering Sea (r = 0.86, the time series of area-averaged SICs not shown), exhibit two notable regimes. That is, SICs are high before 1976 and low after that, corresponding to the 1970s climate regime shift [*Nitta and Yamada*, 1989; *Trenberth*, 1990; *Minobe*, 1997]. The 1970s regime shift is characterized by the strengthening of the Aleutian low [*Nitta and Yamada*, 1989]. This is consistent with negative anomalies of the temporal coefficients for wind after 1976, as the negative anomalies of the temporal coefficients are associated with cyclonic wind anomalies. A wind speed difference map between the two periods (1977–2003 minus 1953–1976) quite resembles the regression map in Figure 4b (not shown). This result indicates that the 1970s climatic regime shift gives the substantial impact on the SIC and wind speed variability in the Bering Sea. The SIC reduction is consistent with *Niebauer* [1998], who reported that the climate regime shift in the 1970s caused a 5% ice cover reduction in the eastern Bering Sea from November to March. Also previous studies showed warming of seawater temperature, decreased ice cover in the Bering Sea [*Niebauer*, 1980; *Luchin et al.*, 2002], and warming of surface air temperature over the Bering Sea [*Bond and Adams*, 2002] and over Alaska [*Minobe*, 2000] in winter in the late 1970s.

[16] Figure 5 shows the second SVD mode in winter. The large SIC anomalies are located around the western part of the shelf break in the northwestern Bering Sea (Figure 5a). This high-SIC anomaly region overlaps western half of the high standard deviations of SIC anomalies shown in Figure 3. The positive SIC anomalies of SVD-2 are consistently accompanied by north-northeasterly and northerly wind anomalies aloft (Figure 5b). Consequently, the high-SIC anomalies of SVD-1 (SVD-2) occupy the eastern (western) parts of the region of high-SIC variability, accompanied by physically consistent wind anomalies.

[17] The temporal coefficients for SIC of SVD-2 exhibit a rapid change from heavy ice year to light ice year in the late 1970s, and the temporal coefficients for wind also indicate a rapid change at the same time (Figure 5c). In contrast to the large and small sea ice regimes in the temporal coefficients of the SVD-1, the temporal coefficients for SIC of SVD-2 do not show a prominent difference before and after 1976/1977. The SICs associated with the SVD-2 were outstandingly large from 1975 to 1977, and were generally large after 1987. Interannual variability of the temporal coefficients for SIC of SVD-2 is larger than that of the temporal coefficients for SIC of SVD-1.

[18] Figure 6 shows the first SVD mode between spring mean (March–May) SICs and February–April mean 1000 hPa wind speeds. The heterogeneous regression map of SIC, which explains 25.3% of the total SIC variance (the heterogeneous regression map accounts for 43.0% of the total SIC variance), indicates large positive amplitudes around the shelf break and the shallow shelf in the northeastern Bering Sea (Figure 6a). This high-SIC area corresponds to the central and eastern parts of the large SIC standard deviations (Figure 3). The location of the high-SIC anomalies of the springtime SVD-1 is reminiscent of those of the wintertime SVD-1, but the high-SIC region of the springtime SVD-1 is wider to the west than that of the wintertime SVD-1 by 9 degrees in longitude.

[19] The spatial pattern of 1000 hPa wind speeds exhibits strong northwesterly and north-northwesterly wind deviations from central to eastern areas over the Bering Sea (Figure 6b). The wind anomalies in these directions were also observed for the wintertime SVD-1. However, the

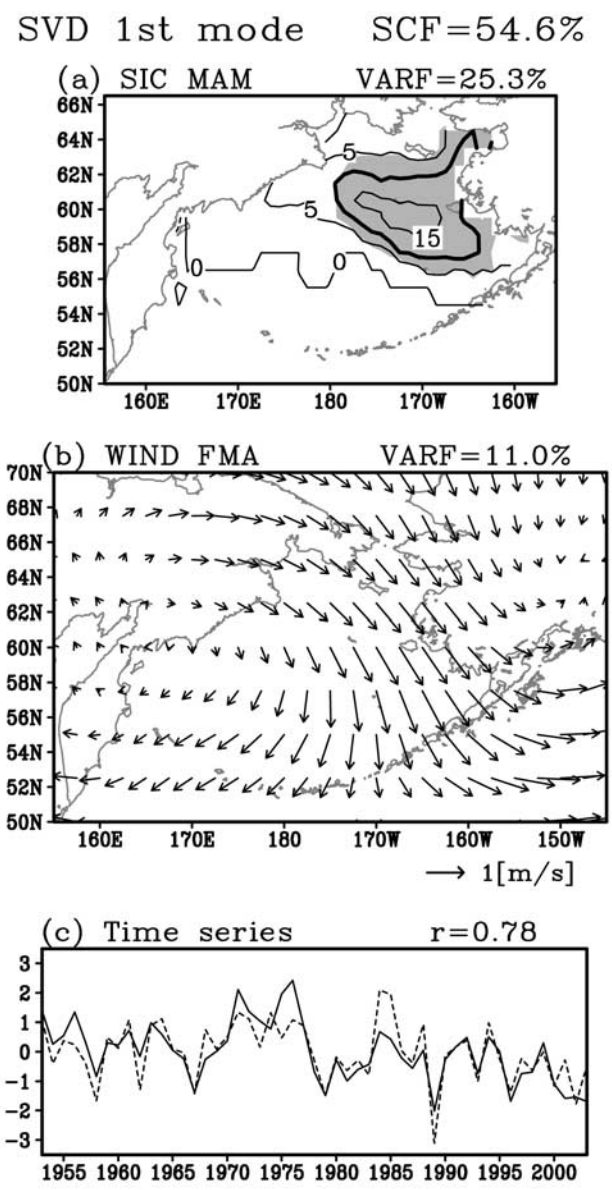

Figure 6. Same as Figure 4, but for the first SVD mode of springtime SICs from March to May and 1 month leading 1000 hPa winds from February to April.

northwesterly wind anomalies in spring prevail on a larger area over the northeastern Bering Sea than the wind anomalies in winter, in association with the westward shift of the center of anticyclonic wind anomalies. This is consistent with the wider sea ice anomalies, and hence the difference of dominant patterns of wind anomalies are most likely to result in the different SIC anomaly distributions between the winter and spring seasons.

[20] The temporal coefficients for SIC of the springtime SVD-1 exhibit less prominent difference between before and after 1976/1977 compared with those of the wintertime SVD-1. Similar to the winter SVD-1, the SIC before 1976 are generally larger than the mean SIC after 1976. However, SICs from 1970 to 1976 are much larger than the SICs before 1970, and hence it may not be appropriate to explain with SIC anomalies before 1976 with a single regime. Consistent with the large SICs from 1970 to 1976 in present analysis, *Minobe* [2002] reported the anomalously cold summertime sea surface temperatures (SSTs) from 1971 to 1976 in the northeastern Bering Sea, and showed that the SSTs are highly correlated with springtime SICs (cold SSTs are associated with larger SICs).

[21] The resemblance in the spatial patterns for the SICs between the wintertime and springtime SVD-1 leads us to ask a question: Do sea ice anomalies in the winter season remain in the spring season? The correlation coefficient between the SIC time series of the springtime SVD-1 and that of the wintertime SVD-1 (SVD-2) is significant at 0.47 (0.30), suggesting that the wintertime SICs variability influences the springtime SICs. This SIC persistency between the winter and spring seasons is not due to the persistency of the atmospheric circulation anomalies or the effect of the wintertime sea ice on springtime wind conditions, because the correlation coefficients between the wind speed time series of springtime SVD-1 and the time series of the leading two wintertime SVD modes are insignificant. Consequently, the SIC anomalies for the springtime SVD-1 are mainly caused by the atmospheric circulation anomalies leading by 1 month, but wintertime SICs play a secondary role.

[22] Figure 7 shows the second SVD mode in spring. The regression coefficients of SIC exhibit large positive amplitudes around the northwestern part of the shelf break (Figure 7a), and this spatial pattern is similar to that of the wintertime SVD-2 (Figure 5a). Consistently, the positive SIC anomalies are accompanied by northerly and north-northeasterly wind anomalies over the western Bering Sea (Figure 7b), associated with the cyclonic circulation anomalies at 54°N, 166°W near Unimak Pass.

[23] The correlation coefficient between temporal coefficients for SIC of the SVD-2 in winter and that in spring is 0.45. This correlation again suggests that sea ice anomalies in winter somewhat affect those in spring.

3.2. Atmospheric Circulation Anomalies

[24] In order to know the relationship between the sea ice variability and large-scale atmospheric circulation, we perform regression analyses of both Z700 and 1000–500 hPa thickness with the temporal coefficients for SIC of the leading two SVD modes both in winter and spring seasons.

[25] Figure 8a shows the regression coefficients of Z700 onto the temporal coefficients for SIC of the SVD-1 in winter for the positive sea ice anomalies. The regressions are characterized by large positive amplitudes over the southern Bering Sea and weaker negative amplitudes of opposing sign centered in western North America. The regression distribution resembles the Pacific North American (PNA) pattern defined by *Wallace and Gutzler* [1981] to some extent. The location of the positive anomalies over the southern Bering Sea suggests a relationship with the Aleutian low variability, and the correlation coefficient between the temporal coefficients for SIC of the wintertime SVD-1 and the November–January mean North Pacific index (NPI), which is an index of the strength of the Aleutian low [*Trenberth and Hurrel*, 1994], is 0.42. The positive Z700 anomalies over the southern Bering Sea yield anticyclonic wind anomalies around the center of the Bering Sea.

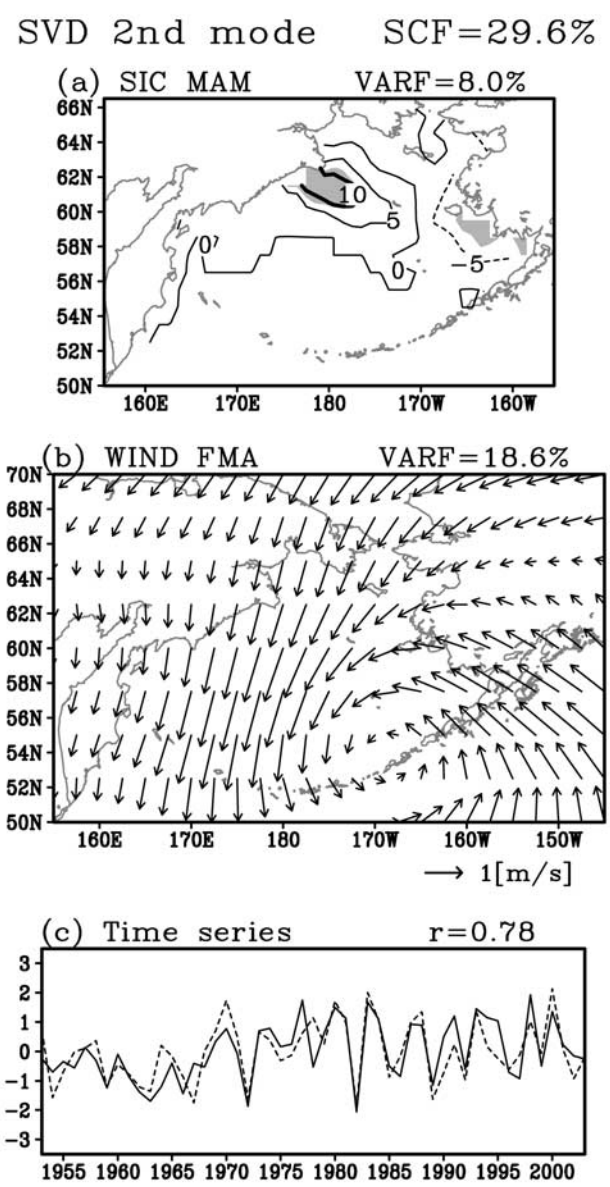

Figure 7. Same as Figure 6, but for the second SVD mode.

[26] The regression coefficients of thickness anomalies of the wintertime SVD-1 shown in Figure 9a exhibit that weak negative thickness anomalies, which indicates negative temperature anomalies in the lower troposphere, are located over the northeastern Bering Sea, where positive sea ice anomalies of the wintertime SVD-1 are located. Yet, the absolute values of corresponding correlation coefficients over the SIC anomalies are small (<0.4). In order to clarify further the importance of the thermodynamics mechanism (ice formation due to heat fluxes) to the sea ice anomalies, we perform regression analyses of SAT with the temporal coefficients for SIC of the SVD-1 in winter (Figure 10). As with thickness anomalies, the negative SAT anomalies are located over the northeastern Bering Sea. Although the SAT anomalies over sea ice may be partly attributed to the sea ice anomalies themselves, the consistency of negative anomalies between thickness and SAT over the northeastern Bering Sea suggests that thermodynamic mechanism contributes to the sea ice anomalies in winter season.

[27] The regression maps of atmospheric circulation for the wintertime SVD-2 indicate different features, compared to those of the wintertime SVD-1. The Z700 regression map for the wintertime SVD-2 exhibits negative anomalies over

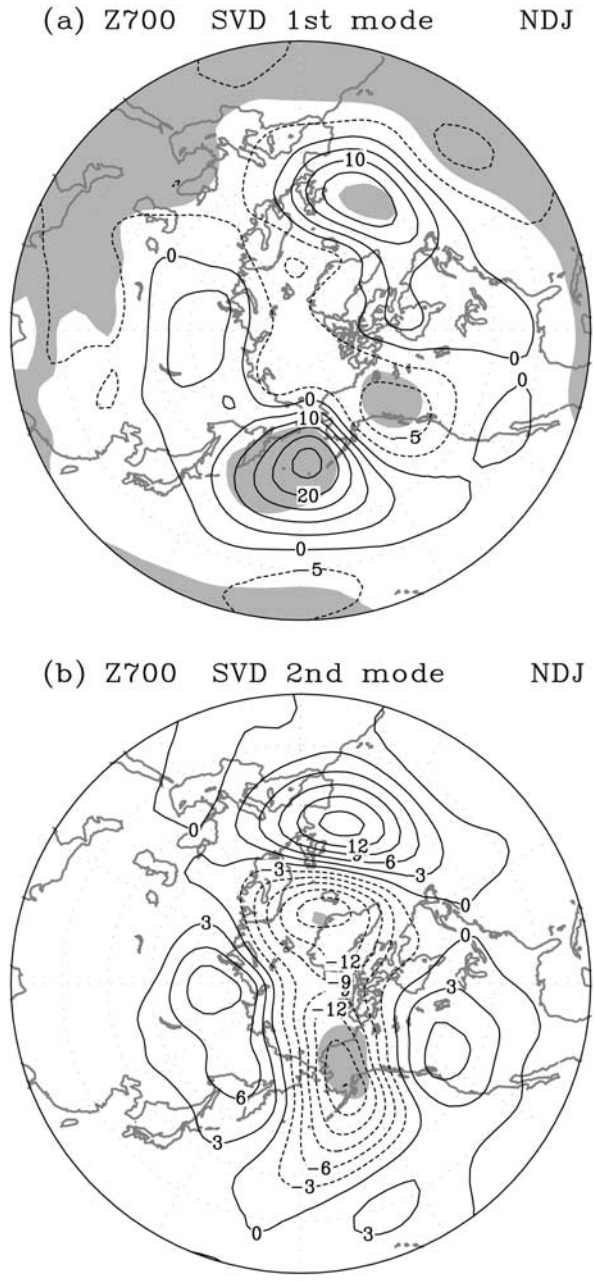

Figure 8. Regression coefficients of 700 hPa geopotential heights at each grid point from November to January onto the temporal coefficients for SIC of the (a) first SVD mode and the (b) second SVD mode in winter in a north polar stereographic map (0°E, and the datelines are in the top and bottom of the panels). The contour interval is 5 m for Figure 8a and 3 m for Figure 8b, and the regions where the absolute values of corresponding correlation coefficients are larger than 0.4 are shaded.

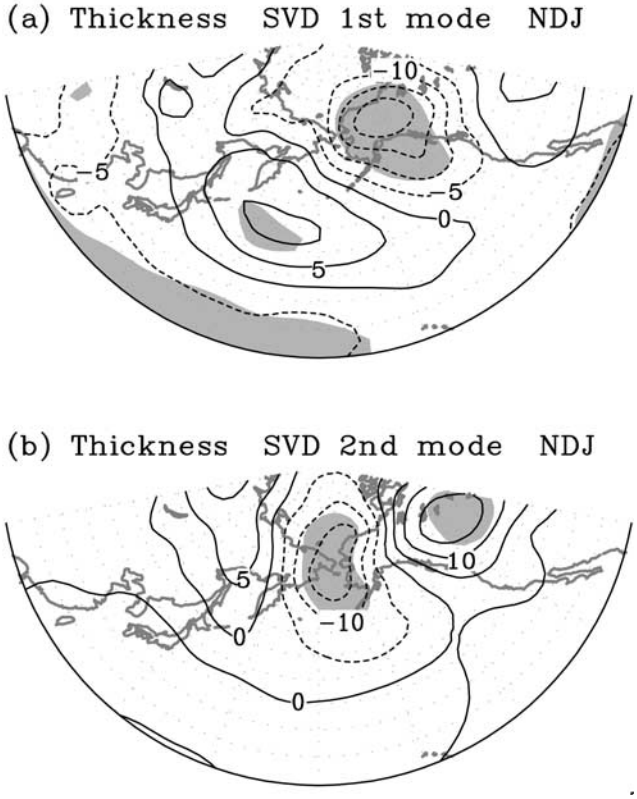

Figure 9. Same as Figure 8, but for 1000–500 hPa thickness. The contour interval is 5 m.

Alaska, and weaker positive anomalies over northeastern Siberia (Figure 8b). The pressure gradients between the negative and the positive anomalies yield the northerly wind anomalies shown in Figure 5b. The anomalously low Z700 over Alaska associated with the larger SICs is consistent with the study of *Fang and Wallace* [1994], who showed that positive 500 hPa anomalies over Alaska due to strong blocking ridge are related to negative sea ice anomalies in the Bering Sea.

[28] The negative thickness anomalies over the northern Bering Sea of the wintertime SVD-2 strongly suggest the contribution of negative temperature anomalies to the positive sea ice anomalies there (Figure 9b). The negative SAT anomalies are also located over the positive sea over the northern Bering Sea (not shown). It is notable that the Z700 and thickness anomalies of the wintertime SVD-1 extend to the low latitudes of the western North Pacific, whereas those of the wintertime SVD-2 are located in the vicinity of the Bering Sea. This result suggests that the atmospheric variability related with wintertime SVD-1 has large scale, whereas atmospheric variability related with the wintertime SVD-2 is relatively local.

[29] Figures 11a and 12a show the regression coefficients of Z700 and 1000–500 hPa thickness, respectively, onto the temporal coefficients for SIC of the springtime SVD-1. The gradients of the Z700 regressions between the large negative anomalies over Alaska and the positive anomalies over northeastern Siberia effectively produce the northwesterly wind anomalies shown in Figure 6a. The large negative thickness anomalies and negative SAT anomalies (SAT map not shown) are located over the northern Bering Sea, consistent with positive sea ice anomalies in the northeastern Bering Sea. It is worthwhile noting that the feature of the large negative Z700 center over Alaska and the negative thickness and SAT anomalies over the northern Bering Sea for the springtime SVD-1 resembles those for the wintertime SVD-2, but the sea ice anomaly locations corresponding to these SVD modes are different. The center position of sea ice anomalies of springtime SVD-1 is located in the northeastern Bering Sea with an eastward shift by 6 degrees in longitude compared with that of the wintertime SVD-2. This difference is probably mainly caused by the difference of the Z700 anomalies over Alaska. The center position of the Z700 anomalies of the springtime SVD-1 is slightly shifted eastward compared to that of the wintertime SVD-2. Consequently, the strong northwesterly (northerly) wind anomalies for the springtime SVD-1 (wintertime SVD-2) are located over the northeastern (northwestern) Bering Sea, which yield positive SIC anomalies there.

[30] The Z700 anomalies corresponding to the springtime SVD-2 shown in Figure 11b exhibit an important similarity with those of the wintertime SVD-1. The Z700 anomalies for the springtime SVD-2 have negative in the southern Bering Sea, with Z700 gradient in the western Bering Sea consistent with the aforementioned northerly wind anomalies (Figure 7b). The large Z700 amplitudes over the southern Bering Sea are commonly found in the wintertime SVD-1 and springtime SVD-2 except for the signs of these anomalies. The correlation coefficient between the temporal coefficients for SIC of the wintertime SVD-2 and the February–April mean NPI is −0.57, which indicates the Z700 variability is related with the Aleutian low. However, the sea ice anomalies of the springtime SVD-2 are located in the northwestern Bering Sea, while those of the wintertime SVD-1 are located in the northeastern Bering Sea. It is noteworthy that the center position of the Z700 anomalies for the springtime SVD-2 is located in the southeastern Bering Sea, but that for the wintertime SVD-1 is observed

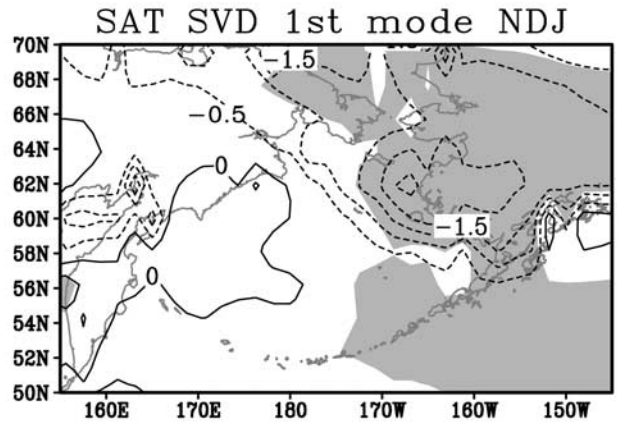

Figure 10. Regression coefficients of surface air temperature at each grid point from November to January onto the temporal coefficients for SIC of the first SVD mode in winter. The contour interval is 0.5°C, and the regions where the absolute values of corresponding correlation coefficients are larger than 0.4 are shaded.

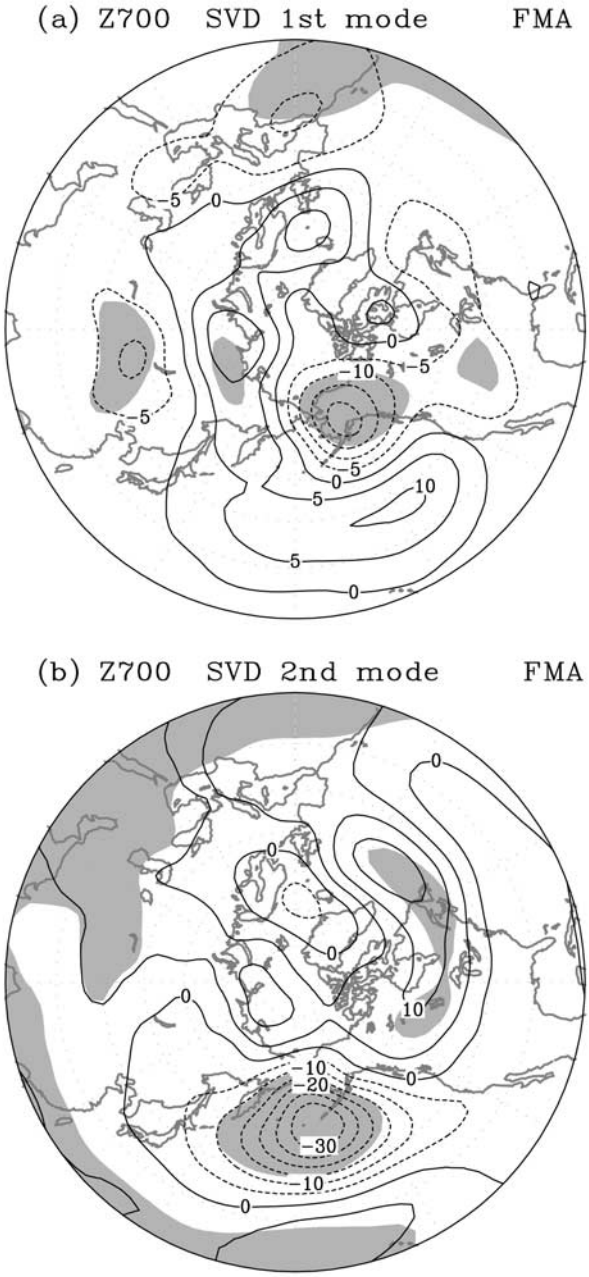

Figure 11. Same as Figure 8, but for data from February to April. The contour interval is 5 m.

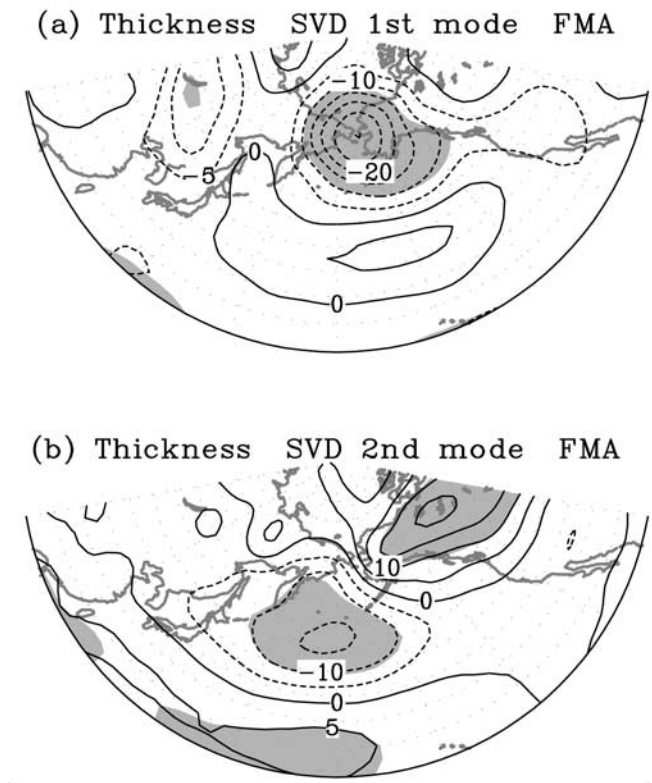

Figure 12. Same as Figure 11, but for 1000–500 hPa thickness. The contour interval is 5 m.

just outside of the Bering Sea with a westward shift by 8 degrees in longitude compared with the springtime SVD-2. The Z700 anomalies for the wintertime SVD-1 (springtime SVD-2) centered in the southern (southeastern) Bering Sea with positive (negative) polarity effectively yield northwesterly (northerly) wind anomalies over the northeastern (northwestern) Bering Sea, which result in positive SIC anomalies there, as mentioned above. Hence this result suggests that slight difference of the center position of Z700 anomalies significantly affects the location and sign of sea ice anomalies in the Bering Sea.

[31] The spatial pattern of 1000–500 hPa thickness anomalies of the springtime SVD-2 shown in Figure 12b resembles that of the wintertime SVD-1, but the anomalies of the springtime SVD-2 over the northwestern North Pacific are large compared with those of the wintertime SVD-1. The absolute values of correlation coefficients in the northwestern Bering Sea, where positive sea ice anomalies of the springtime SVD-2 are located, are small (<0.4). This result suggests the contribution of the thermodynamic mechanism for the sea ice variability is small. The corresponding SAT pattern shown in Figure 13 exhibits negative anomalies over the positive sea ice anomalies. However, because these negative anomalies do not correspond to the negative thickness anomalies aloft and are

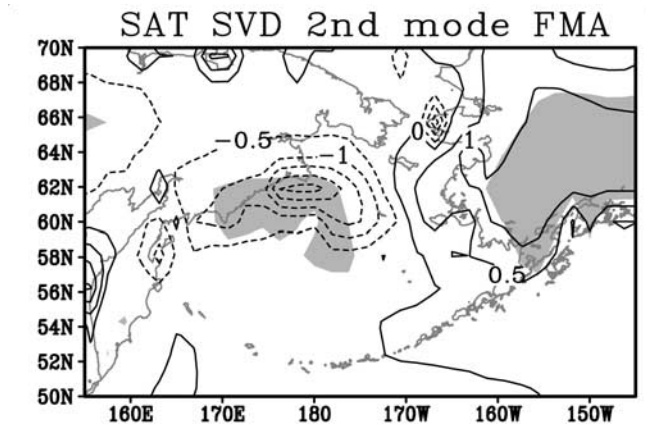

Figure 13. Same as Figure 10, bur for data from February to April and the second SVD mode in spring.

localized over the positive sea ice anomalies, the SAT anomalies are probably largely affected by sea ice anomalies themselves, i.e., a sea ice feedback to the local SAT [*Wu et al.*, 2004]. Hence it is confirmed that the contribution of SAT for sea ice variability again can be ignored in spring season, during which the ocean melting process may be important.

4. Summary and Discussion

[32] In this paper, we investigated the interannual variability of sea ice in the Bering Sea and its relationship to 1000 hPa wind speeds using SVD analyses, and the statistically significant two SVD modes are documented in the winter and spring seasons. The region of high year-to-year SIC variability is predetermined by bathymetries, and is limited to the shelf break and the shallow shelf. In this region, 1 month leading local wind anomalies strongly contribute to the SIC anomalies, with a relation that the northerly or northwesterly wind anomalies increase the SICs. The first (second) SVD mode explains the SIC variability in the northeastern (northwestern) Bering Sea, associated with the local northwesterly (northerly) wind anomalies for the positive SIC anomalies. The relation between the SIC and wind anomalies are consistent with the dynamic (sea ice drift) and thermodynamic (ice formation due to heat flux) mechanisms. These features are common in the winter and spring seasons. Consequently, the location of SIC variability is strongly constrained by the topography, and the detailed structures of SIC anomalies are determined by local winds.

[33] In association with the SIC anomalies of the leading two SVD modes in the winter and spring seasons, the relation between sea ice and atmospheric circulation anomalies indicates that the wintertime SVD-1 and springtime SVD-2 are related with large-scale atmospheric variability extended to the low latitude of the western North Pacific, whereas the wintertime SVD-2 and springtime SVD-1 are related with relatively local atmospheric variability confined to the middle and high latitudes. The large-scale atmospheric variability is characterized by the association with the Aleutian low variations. On the other hand, the local atmospheric variability is characterized by the large Z700 anomalies over Alaska, and the large temperature anomalies over the northern Bering Sea. Because the Aleutian low in spring is weaker than that in winter, it is consistent that the large-scale atmospheric variability in spring explains smaller sea ice fluctuations than that in winter.

[34] A comparison of the Z700 anomalies between the wintertime SVD-1 and springtime SVD-2 shows that a subtle difference of the center position of Z700 anomalies results in the substantial difference of the sea ice responses in the Bering Sea. The center of the Z700 for the wintertime SVD-1 is located to the slightly westward of that for the springtime SVD-2 over the southern Bering Sea, resulting in effective geopotential height gradients and hence wind anomalies in the northeastern (northwestern) Bering Sea for the wintertime SVD-1 (springtime SVD-2). Again, the wintertime SVD-2 and springtime SVD-1 have the negative Z700 anomalies over Alaska, but the location of the corresponding sea ice anomalies is different between these two modes. The difference of the center position of the Z700 anomalies over Alaska probably causes the difference location and direction of wind anomalies over the Bering Sea. These results suggest understanding of the wind anomalies over the Bering Sea is important to understanding of the year-to-year sea ice variability. It is not clear why these slight differences of atmospheric fluctuations between winter and spring seasons occur, but the cause of the seasonal dependency of the atmospheric fluctuations is beyond the scope of this paper.

[35] Which mechanism (dynamics or thermodynamics) is important in the interannual variability remains an open question. We calculate a wind-driven ice advection distance. For example, if sea ice floes drift at about 4% of the 1 m s^{-1} wind speed anomalies for 3 months, sea ice floes advect about 3 degrees in latitude [*Reynolds et al.*, 1985]. This anomalous drift distance combined with the climatological SIC distributions shown in Figure 2 is large enough for the observed SIC anomalies. Thus the dynamic mechanism can solely explain the sea ice variability captured in the present analysis. On the other hand, the estimation of the contribution of the thermodynamic mechanism to the interannual variability needs reliable surface heat flux and sea ice thickness data [e.g., *Tateyama and Enomoto*, 2001] over the Bering Sea. It is desirable to investigate the role of the dynamic and thermodynamic mechanisms in sea ice variations using numerical coupled ocean and ice models in the future.

[36] It is interesting how the global warming influences the sea ice in the Bering Sea via the atmospheric circulation anomalies. *Carnell and Senior* [1998] showed wintertime SLP decreases around the southeastern Bering Sea in a doubled-CO_2 simulation with the second Hadley Centre coupled ocean-atmosphere general circulation model. If this is the case, the SLP anomalies and associated wind anomalies may be less effective to sea ice over the northeastern Bering Sea, but cause northerly wind anomalies and tend to increase sea ice over the northwestern Bering Sea opposing to the sea ice decrease tendency due to warming itself. Therefore in order to understand the future sea ice variability in the Bering Sea, it is important to accurately know the variations of atmospheric circulation anomalies.

[37] **Acknowledgments.** This study was supported by grant-in-aid for scientific research (kaken-hi 15540417 to S.M.) and by 21st Century Center of Excellence Program on "Neo-Science of Natural History" led by H. Okada (to S.M.), both from the Ministry of Education, Culture, Sports, Science and Technology, Japan. Constructive comments from three reviewers have been helpful in improving this paper. Some figures have been produced with the GrADS package developed by B. Doty.

References

Bond, N. A., and J. M. Adams (2002), Atmospheric forcing of the southeast Bering Sea Shelf during 1995–99 in the context of a 40-year historical record, *Deep Sea Res., Part II*, *49*, 5869–5887.

Bretherton, C. S., C. Smith, and J. M. Wallace (1992), An intercomparison of methods for finding coupled patterns in climate data, *J. Clim.*, *5*, 541–560.

Carnell, R. E., and C. A. Senior (1998), Changes in mid-latitude variability due to increasing greenhouse gases and sulphate aerosols, *Clim. Dyn.*, *14*, 369–383.

Cavalieri, D. J., and C. L. Parkinson (1987), On the relationship between atmospheric circulation and the fluctuations in the sea-ice extents of the Bering and Okhotsk Seas, *J. Geophys. Res.*, *92*, 7141–7162.

Cavalieri, D. J., C. L. Parkinson, P. Gloersen, J. C. Comiso, and H. J. Zwally (1999), Deriving long-term time series of sea ice cover from satellite passive-microwave multisensor data sets, *J. Geophys. Res.*, *104*, 15,803–15,814.

Deser, C., J. E. Walsh, and M. S. Timlin (2000), Arctic sea ice variability in the context of recent atmospheric circulation trends, *J. Clim.*, *13*, 617–633.

Fang, Z.-F., and J. M. Wallace (1994), Arctic sea ice variability on a timescale of weeks and its relation to atmospheric forcing, *J. Clim.*, *7*, 1897–1914.

Fang, Z.-F., and J. M. Wallace (1998), North-Pacific sea ice and Kuroshio SST variability and its relation to the winter monsoon, *Pol. Meteorol. Glaciol.*, *12*, 58–67.

Grumbine, R. W. (1996), Automated passive microwave sea ice concentration analysis at NCEP, U.S. Dept. of Commerce, NCEP technical note, Natl. Weather Serv., Natl. Oceanic and Atmos. Admin., Camp Springs, Md.

Hunt, G. L., Jr., and P. J. Stabeno (2002), Climate change and the control of energy flow in the southeastern Bering Sea, *Prog. Oceanogr.*, *55*, 5–22.

Kalnay, E., et al. (1996), The NCEP/NCAR 40-year reanalysis project, *Bull. Am. Meteorol. Soc.*, *77*, 437–472.

Kimura, N., and M. Wakatsuchi (2000), Relationship between sea-ice motion and geostrophic wind in the Northern Hemisphere, *Geophys. Res. Lett.*, *27*, 3735–3738.

Kimura, N., and M. Wakatsuchi (2001), Mechanisms for the variation of sea ice extent in the Northern Hemisphere, *J. Geophys. Res.*, *106*, 31,319–31,331.

Luchin, V. A., I. P. Semiletov, and G. E. Weller (2002), Changes in the Bering Sea region: Atmosphere-ice-water system in the second half of the twentieth century, *Prog. Oceanogr.*, *55*, 23–44.

Minobe, S. (1997), A 50–70 year climatic oscillation over the North Pacific and North America, *Geophys. Res. Lett.*, *24*, 683–686.

Minobe, S. (2000), Spatio-temporal structure of the pentadecadal variability over the North Pacific, *Prog. Oceanogr.*, *47*, 381–408.

Minobe, S. (2002), Interannual to interdecadal changes in the Bering Sea and concurrent 1998/99 changes over the North Pacific, *Prog. Oceanogr.*, *55*, 45–64.

Niebauer, H. J. (1980), Sea ice and temperature variability in the eastern Bering Sea and the relation to atmospheric fluctuations, *J. Geophys. Res.*, *85*, 7507–7515.

Niebauer, H. J. (1998), Variability in Bering Sea ice cover as affected by a regime shift in the North Pacific in the period 1947–1996, *J. Geophys. Res.*, *103*, 27,717–27,737.

Niebauer, H. J., V. Alexander, and S. Henrichs (1990), Physical and biological oceanographic interaction in the spring bloom at the Bering Sea marginal ice edge zone, *J. Geophys. Res.*, *95*, 22,229–22,241.

Nitta, T., and S. Yamada (1989), Recent warming of tropical sea surface temperature and its relationship to the Northern Hemisphere circulation, *J. Meteorol. Soc. Jpn.*, *67*, 375–383.

Overland, J. E., and C. H. Pease (1982), Cyclone climatology of the Bering Sea and its relation to sea ice extent, *Mon. Weather Rev.*, *110*, 5–13.

Parkinson, C. L. (1991), Interannual variability of the spatial distribution of sea ice in the north polar region, *J. Geophys. Res.*, *96*, 4791–4801.

Parkinson, C. L., and D. J. Cavalieri (2002), A 21 year record of Arctic sea-ice extents and their regional, seasonal and monthly variability and trends, *Ann. Glaciol.*, *34*, 441–446.

Rayner, N. A., D. E. Parker, E. B. Horton, C. K. Folland, L. V. Alexander, D. P. Rowell, E. C. Kent, and A. Kaplan (2003), Global analyses of sea surface temperature, sea ice, and night marine air temperature since the late nineteenth century, *J. Geophys. Res.*, *108*(D14), 4407, doi:10.1029/2002JD002670.

Reynolds, M., C. H. Peace, and J. E. Overland (1985), Ice drift and regional meteorology in the southern Bering Sea: Results from MIZEX west, *J. Geophys. Res.*, *90*, 11,967–11,981.

Saitoh, S., T. Iida, and K. Sasaoka (2002), A description of temporal and spatial variability in the Bering Sea spring phytoplankton blooms (1997–1999) using satellite multi-sensor remote sensing, *Prog. Oceanogr.*, *55*, 131–146.

Springer, A. M., C. P. McRoy, and M. V. Flint (1996), The Bering Sea Green Belt: Shelf-edge processes and ecosystem production, *Fish. Oceanogr.*, *5*, 205–223.

Stabeno, P. J., N. A. Bond, N. B. Kachel, S. A. Salo, and J. D. Schumacher (2001), On the temporal variability of the physical environment over the southeastern Bering Sea, *Fish. Oceanogr.*, *10*, 81–98.

Tateyama, K., and H. Enomoto (2001), Observation of sea-ice thickness fluctuation in the seasonal ice-covered area during 1992–99 winters, *Ann. Glaciol.*, *33*, 449–456.

Trenberth, K. E. (1990), Recent observed interdecadal climate changes in the Northern Hemisphere, *Bull. Am. Meteorol. Soc.*, *71*, 988–993.

Trenberth, K. E., and J. W. Hurrel (1994), Decadal atmosphere-ocean variations in the Pacific, *Clim. Dyn.*, *9*, 303–319.

Venegas, S. A., L. A. Mysak, and D. N. Straub (1997), Atmosphere-ocean coupled variability in the South Atlantic, *J. Clim.*, *10*, 2904–2920.

Wallace, J. M., and D. S. Gutzler (1981), Teleconnections in the geopotential height field during the Northern Hemisphere winter, *Mon. Weather Rev.*, *109*, 784–812.

Walsh, J. E., and W. L. Chapman (2001), 20th-century sea-ice variations from observational data, *Ann. Glaciol.*, *33*, 444–448.

Walsh, J. E., and C. M. Johnson (1979), An analysis of Arctic sea ice fluctuations, 1953–77, *J. Phys. Oceanogr.*, *9*, 580–591.

Walsh, J. E., and J. E. Sater (1981), Monthly and seasonal variability in the ocean-ice-atmosphere systems of the North Pacific and the North Atlantic, *J. Geophys. Res.*, *86*, 7425–7445.

Wang, J., and M. Ikeda (2000), Arctic Oscillation and Arctic Sea-Ice Oscillation, *Geophys. Res. Lett.*, *27*, 1287–1290.

Wu, B., J. Wang, and J. E. Walsh (2004), Possible feedback of winter sea ice in the Greenland and Barents Seas on the local atmosphere, *Mon. Weather Rev.*, *132*, 1868–1876.

S. Minobe and N. Y. Sasaki, Division of Earth and Planetary Sciences, Graduate School of Science, Hokkaido University, Sapporo, 060-0810, Japan. (minobe@ep.sci.hokudai.ac.jp; sasa@ep.sci.hokudai.ac.jp)